Thermodynamic comparison of solar methane reforming via catalytic and redox cycle routes

Solar Energy 215 (2021) 169–178

Contents lists available at ScienceDirect

Solar Energy

journal homepage: www.elsevier.com/locate/solener

Thermodynamic comparison of solar methane reforming via catalytic and redox cycle routes

B. Bulfin [a,*], S. Ackermann [b], P. Furler [b], A. Steinfeld [a]

[a] Department of Mechanical and Process Engineering, ETH Zürich, 8092 Zürich, Switzerland
[b] Synhelion SA, Via Cantonale 19, 6900 Lugano, Switzerland

ARTICLE INFO

Keywords:
Solar methane reforming
Concentrated solar energy
Solar fuels
Thermochemical redox cycles

ABSTRACT

Thermochemical methane reforming to syngas is performed on a massive scale in the chemical industry, providing feedstock for many chemical processes such as hydrogen, ammonia and methanol production. The high temperature process heat required for the endothermic reforming reaction could be supplied by conentrated solar energy, in a hybrid solar-fossil process. This can be achieved by re-designing conventional reforming technologies to utilize solar energy as the heat source. Another possible approach is to use a two-step metal oxide redox cycle. Here we compare the two solar thermochemical reforming routes, namely redox reforming and catalytic reforming using thermodynamic analysis and discuss the prospects for both technologies with a focus on methane conversion extents, syngas composition, and energy conversion efficiencies. Further processing of the syngas to liquid fuels is also discussed, in order to highlight how these processes can fit together with gas-to-liquids technologies. The analysis highlights that the redox cycle approach could produce a higher quality syngas, but at the expense of additional thermodynamic constraints, which are sensitive to carbon formation, and also lead to a greater energy demand relative to catalytic reforming.

1. Introduction

Direct methane reforming is described by the endothermic reactions,

$$CH_4 + H_2O \rightarrow CO + 3H_2 \qquad \Delta h^{\circ}_{1173\ K} = 218\ [kJ\,mol^{-1}] \tag{1}$$

$$CH_4 + CO_2 \rightarrow 2CO + 2H_2 \qquad \Delta h^{\circ}_{1173\ K} = 259\ [kJ\,mol^{-1}] \tag{2}$$

known as wet and dry reforming respectively. Current industrial hydrogen production plants utilize wet reforming, performed over a catalyst at temperatures in the region of 700–900 °C with excess of steam to avoid coking. This produces hydrogen rich syngas, which can be further enriched via the water gas shift reaction,

$$CO + H_2O \leftrightarrow CO_2 + H_2, \qquad \Delta h^{\circ} = -41\ [kJ\,mol^{-1}]. \tag{3}$$

which is slightly exothermic. Conventionally the required heat is supplied externally by the combustion of a portion of the feedstock and of the tail gas after down-stream processing of the syngas, which evidently reduces product yield and releases greenhouse gases.

In this work we consider downstream conversion of our syngas to liquid fuels. Fischer–Tropsch synthesis often requires a syngas composition in the region of $2H_2$:1CO. Dry reforming can help obtain such a ratio, but it is problematic due to coke formation, deactivating the catalyst (Muraza and Galadima, 2015). On the other hand, combined dry and wet (mixed) reforming with a controlled content of CO_2 in the feedstock can be used to adjust the syngas composition, which has been used for methanol production (Bartholomew and Farrauto, 2011; Rostrup-Nielsen et al., 2002). This has been implemented on an industrial scale at a gas-to-liquids (GTL) plant, where the CO_2 required was available from a near-by ammonia synthesis plant (Holm-Larsen, 2001). The mixed reforming process in this case requires higher temperatures (950 °C) than steam-based reforming to ensure conversion of CO_2 (Bartholomew and Farrauto, 2011).

Rather than combusting part of the natural gas feedstock to provide heat for these reforming processes, the heat of reaction could be supplied by concentrated solar energy, offering a means of converting solar to chemical energy (Romero and Steinfeld, 2012; Zedtwitz et al., 2006). Solar driven reforming has been extensively studied (Segal and Epstein, 2003; Berman et al., 2007; Diver et al., 1992; Buck et al., 1991; Muir et al., 1994), with two recent reviews on these research efforts, which offer valuable insight into the routes available to achieve solar reforming (Agrafiotis et al., 2014; Sheu et al., 2015). The core development

* Corresponding author.
E-mail address: bulfinb@ethz.ch (B. Bulfin).

https://doi.org/10.1016/j.solener.2020.11.076
Received 5 June 2020; Received in revised form 19 November 2020; Accepted 28 November 2020
Available online 11 January 2021

required is to find a practical engineering solution to solarize the already established technologies of methane reforming.

In recent years a growing number of researchers have focused their attention on a redox cycle route to methane reforming (Warren et al., 2017; Welte et al., 2017; Nair and Abanades, 2016; He et al., 2014; Kodama et al., 2000; Krenzke et al., 2016; Fosheim et al., 2019),

$$CH_4 + M_yO_x \overset{\text{endothermic}}{\longrightarrow} M_yO_{x-1} + CO + 2H_2 \quad (4)$$

$$M_yO_{x-1} + H_2O/CO_2 \overset{\text{exothermic}}{\longrightarrow} M_yO_x + H_2/CO. \quad (5)$$

The first reaction involves reducing the oxide in an endothermic reaction, using methane as a reducing agent, and the second reaction closes the cycle via an exothermic oxidation under steam or carbon dioxide. Reaction 1 has been previously proposed for combining the reduction of metal oxides with the reforming of methane for the co-production of metal and syngas using solar process heat (Steinfeld et al., 1993; Steinfeld and Thompson, 1994; Steinfeld et al., 1995; Halmann et al., 2002; Steinfeld et al., 1998). Fig. 1 shows a simple schematic of this process compared to conventional catalytic reforming. A number of metal oxides have been investigated for redox reforming including ceria (Welte et al., 2017; Otsuka et al., 1993; Otsuka et al., 1998; Krenzke and Davidson, 2014), iron oxides (Steinfeld et al., 1993; Steinfeld, 1997; He et al., 2014), zinc oxide (Steinfeld et al., 1995; Kräupl and Steinfeld, 2001), and perovskites (He and Li, 2015). It has been highlighted in the literature that by using a redox material with a strong oxygen affinity such as CeO_2, full dry reforming is possible (Warren et al., 2017). In this way one may have more flexibility in tuning the composition of the syngas than in catalytic reforming.

In this work we present a thermodynamic analysis of direct solar catalytic reforming and redox reforming with the metal oxides CeO_2, Fe_3O_4, FeO, and ZnO, focusing on the methane conversion extent, as well as on the syngas composition and its suitability for further gas to liquid processes. All reforming processes were modelled at pressure of 15 bar (often used in industrial reforming), setting this work aside from most previous analysis of redox reforming, which have been at 1 bar (Warren et al., 2017; Steinfeld et al., 1993; Steinfeld et al., 1995). This is an important distinction as the pressure has a considerable effect on the methane conversion extents. One recent study by Holzemer-Zerhusen et al. (2020), does indeed investigate higher pressures, but with an analysis that is more consistent with a co-feeding reactor, which would require moving particles of the oxide. The analysis presented here is more suitable for a fixed bed isothermal system, which is practically feasible and commonly applied in the chemical industry.

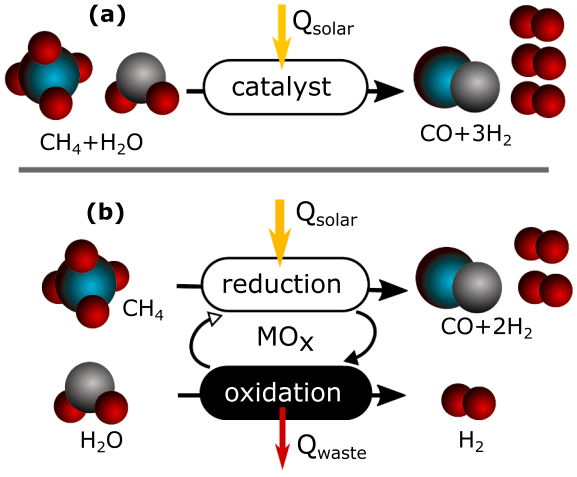

Fig. 1. A schematic showing the two routes for methane reforming **(a)** catalytic reforming and **(b)** redox reforming. Both cases have the same feedstock and products, and are powered by solar energy, but the redox route has a larger heat requirement and thus a waste heat component released during the exothermic oxidation reaction.

2. Thermodynamic modelling

In the following analysis we assume that the conversion extent is not kinetically limited and that the system is in thermodynamic equilibrium.

Thermodynamics of the gas phase species and solid carbon were modelled using the software cantera (Goodwin et al., 2017), and the *GRI-MECH 3.0* database. Thermodynamic for the metals and oxides Fe_3O_4, FeO, Fe, ZnO, and Zn were modelled using Factsage (Bale et al., 2009; Bale et al., 2002), and for ceria the relevant thermodynamic data was obtained from Bulfin et al. (2016).

Fig. 2 shows Ellingham diagrams for methane reforming reactions in the upper graph. From this we can see that wet and dry reforming become favourable at temperatures above 900 K. In the case of thermochemical methane reforming we must consider methane reduction of the metal oxides given by,

$$CH_4 + \frac{1}{\delta_{red} - \delta_{ox}} CeO_{2-\delta_{ox}} \rightarrow \frac{1}{\delta_{red} - \delta_{ox}} CeO_{2-\delta_{red}} + CO + 2H_2 \quad (6)$$

$$CH_4 + Fe_3O_4 \rightarrow 3FeO + CO + 2H_2 \quad (7)$$

$$CH_4 + ZnO \rightarrow Zn + CO + 2H_2. \quad (8)$$

Note, that ceria undergoes non-stoichiometric reduction and oxidation, and thus we introduce δ as the extent of non-stoichiometry. The change in Gibbs free energy (ΔG) for these reactions are also shown in Fig. 2. Reduction of Fe_3O_4 to FeO is favourable at temperatures above 900 K, but reduction of ZnO to Zn and CeO_2 to $CeO_{1.9}$ requires higher temperatures in the region of 1100 K.

The splitting of CO_2 (or H_2O) with the reduced oxides is given by the equations,

$$\frac{1}{\delta_{red} - \delta_{ox}} CeO_{2-\delta_{red}} + CO_2 \rightarrow \frac{1}{\delta_{red} - \delta_{ox}} CeO_{2-\delta_{ox}} + CO \quad (9)$$

$$3FeO + CO_2 \rightarrow Fe_3O_4 + CO \quad (10)$$

$$Zn + CO_2 \rightarrow ZnO + CO. \quad (11)$$

The right graph in Fig. 2 shows the ΔG for these reactions, where both Zn and $CeO_{1.9}$ favourably split CO_2 at all temperatures plotted. However, FeO does not favourably split CO_2 until below 850 K. This is a limitation of thermochemical redox cycles; if the metal oxide easily gives up its oxygen, it will conversely offer a lower yield when splitting H_2O or CO_2, as is the case with the Fe_3O_4-FeO redox pair. However, FeO itself can also be reduced to Fe, which is included in the latter analysis.

During catalytic reforming, or the methane reduction step of redox reforming, an unwanted side reaction is methane cracking,

$$CH_4 \rightarrow C(s) + H_2. \quad (12)$$

The equilibrium composition of this reaction for pure methane at 15 bar is given in the ESI, where it can be seen that this reaction is also favourable at the conditions considered. We therefore include solid phase carbon in our thermodynamic analysis.

In order to get a complete picture of the thermodynamics we must use a more robust chemical equilibrium analysis. For catalytic methane reforming, given a starting composition with one mole of methane and set amounts of steam and carbon dioxide the reaction, given by the following equation,

$$CH_4 + a_1H_2O + a_2CO_2 \overset{T,P}{\rightarrow} x_1CH_4 + x_2CO + x_3H_2 + x_4H_2O + n_CC(s) + ... \quad (13)$$

can be solved to find the gas mole fractions x_i's and the number of moles of solid phase carbon n_C, which minimize the Gibbs free energy of the

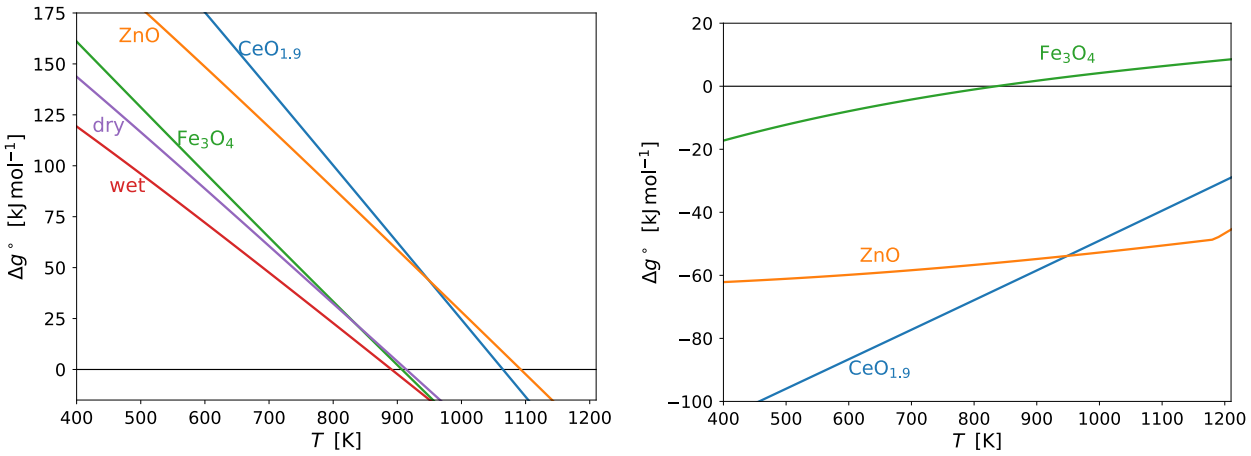

Fig. 2. Ellingham diagrams of methane reforming reactions, with the molar change in Gibbs free energy Δg vs. T. **Left:** Wet and dry reforming given in Eqs. (1) and (2), and redox reforming given in Eqs. (6)–(8). **Right:** CO_2 splitting according to Eqs. (9)–(11).

system. This was performed using cantera, which uses an element potential method to equilibrate an initially defined mixture of gases (Smith, 1982). This method is appropriate here as in a catalytic reactor the gases are fed in a defined stoichiometric ratio.

In the case of redox reforming we must consider the reactions between solid phase oxides and gaseous methane, and in the oxidation step steam and carbon dioxide. There are two distinct approaches to modeling the thermodynamic equilibrium of such a reaction, which are illustrated in Fig. 3.

- **(a) Ideal stoichiometric model:** minimize the Gibbs free energy of the solid and gas with the ideal stoichiometric ratio of reactants at a given temperature and pressure.
- **(b) Oxygen activity model:** determine the chemical potential of oxygen μ_{O_2} in the metal oxide and then minimize the molar Gibbs free energy of the gas phase at constant temperature, pressure and oxygen chemical potential.

The ideal stoichiometric approach **(a)** is the standard approach to determining equilibrium composition that has been used for these reactions in previous analysis (Steinfeld et al., 1995; Steinfeld et al., 1993). However, realizing such a system in a thermochemical redox reactor is not straightforward, because a batch reactor containing stoichiometric mixtures would be highly impractical. Another way to achieve such ideal stoichiometric mixtures would be co-feeding the solid and gaseous reactants into a continuous reactor, which would involve complex moving particle reactor systems. Fixed bed reactors are more commonly applied in chemical looping processes, but in this configuration the large difference in density between the solid and gas phases, means that the gas entering the reactor will come into contact with the solid, such that the solid reactant is available in excess. Over a complete cycle we could supply the ideal stoichiometric amount of gas, but the solid will still be locally in excess as the reaction is taking place. This can result in further oxidation of the syngas via the reactions,

$$CO + M_yO_x \rightarrow M_yO_{x-1} + CO_2 \quad (14)$$

$$H_2 + M_yO_x \rightarrow M_yO_{x-1} + H_2O \quad (15)$$

which is underestimated by the ideal stoichiometric model, as the oxide is in limited supply. To more accurately model a fixed bed reactor system we need to use another approach.

The oxygen activity model **(b)** assumes that the gaseous reactants will come into contact with the solid phase oxide in excess, so that excess oxygen will be available, but only at the intrinsic oxygen chemical potential of the oxide reduction reaction. This is then a phase equilibrium calculation, where we find the gas phase composition that would be in equilibrium with the solid, according to the chemical potential of oxygen in the oxide. The stoichiometry in this model is not fixed, but it is determined by assuming that only enough oxide is present to supply the oxygen taken up by the gas. As we shall see later, this approach is very useful in determining selectivity towards syngas for redox reforming, where the result only depends on the intrinsic oxygen thermodynamics of the solid oxide. This modelling approach is also closer in nature to the type of fixed bed experimental demonstrations that have been reported in the literature. In these experimental demonstrations selectivity can be an issue due to the formation of CO_2 and H_2O (Warren et al., 2017; Steinfeld et al., 1993; Kang et al., 2008), something which is not predicted by the stoichiometric model. Therefore, the results presented for redox reforming in this work follow this oxygen activity approach, as it highlights these selectivity issues.

Modelling the system according to case **(b)** can be achieved in two ways. The first method is to use a fixed stoichiometry as in case **(a)**, but with the oxide in enough excess to fully oxidize methane to CO_2 and H_2O. For example $3Fe_3O_4$:$1CH_4$, in which case oxygen will move to the gas phase until the chemical potential of oxygen in the gas and the solid are equal. This method is suitable for the iron and zinc cycles, where we

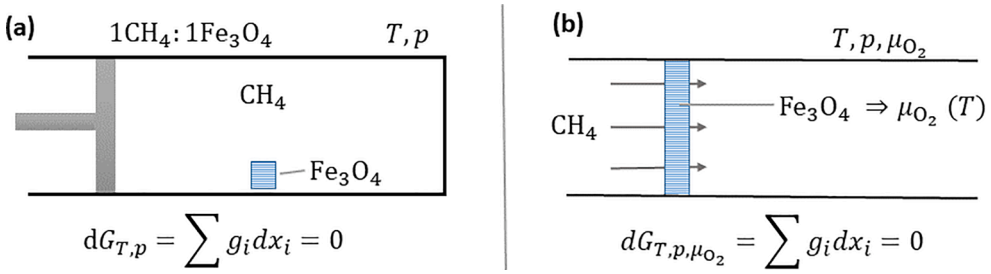

Fig. 3. A schematic illustrating the concept of the two different chemical equilibrium approaches which can be applied.

have a defined stoichiometry. To close the cycles mass balance, we then neglect the unreacted metal oxide as in practice additional methane could be passed through the reactor until the oxide is fully reacted.

The second method is by treating the methane reduction of a metal oxide as the sum of thermal dissociation of the metal oxide,

$$M_yO_x \rightarrow M_yO_{x-1} + \frac{1}{2}O_2 \tag{16}$$

and partial oxidation of methane

$$CH_4 + aO_2 \overset{T,P}{\rightarrow} x_1CH_4 + x_2CO + x_3H_2 + x_4H_2O + x_5CO_2 + n_CC(s) + \ldots\ldots \tag{17}$$

The oxygen chemical potential, or equivalent oxygen partial pressure assuming ideal gas behaviour, during the reduction reaction given in Eq. (16) can be determined from the equilibrium equation,

$$\Delta h_O - T\Delta s_O = -\frac{1}{2}RT\ln\left(\frac{p_{O_2}}{p^\circ}\right). \tag{18}$$

We can then use cantera to determine the equilibrium of the CH_4 partial oxidation reaction given in Eq. (17), varying the parameter a until the oxygen partial pressure matches that determined from Eq. (18), for the reduction of the metal oxide. This would be the equilibrium gaseous mixture for methane reduction of the metal oxide at the given temperature, pressure and oxygen partial pressure. It is then assumed that we only use enough metal oxide to supply the oxygen to reach this equilibrium, and no further excess. This method is well suited to analysing ceria redox reforming, where we can now determine the gas phase equilibrium as a function of non-stoichiometry δ, as explained below.

The re-oxidation of the metal oxide can be solved using the same oxygen activity method and considering the reactions

$$H_2O \overset{T,p}{\rightarrow} x_1H_2 + x_2O_2 + x_3H_2O + \ldots\ldots \tag{19}$$

$$CO_2 \overset{T,p}{\rightarrow} x_1CO + x_2O_2 + x_3CO_2 + n_CC(s) + \ldots\ldots \tag{20}$$

In this case the amount of oxidant (H_2O/CO_2) that will allow for complete re-oxidation of the metal oxide must be calculated based on the conversion extent of the oxidants. During CO_2 splitting the formation of solid carbon can also be thermodynamically favourable. This has been experimentally observed by Ehrensberger et al. for the reduction of CO_2 using iron (Ehrensberger et al., 1997). They used a closed reactor system and found that first carbon monoxide formed, followed by a much slower rate of solid carbon formation. There results indicate it would be kinetically limited in a continuous flow reactor at the same conditions, but it is still valuable to see where it is thermodynamically possible, in case it needs to be avoided.

Ceria introduces an additional complexity in that it undergoes partial reduction,

$$CeO_2 \overset{T,p_{O_2}}{\rightarrow} CeO_{2-\delta} + \frac{\delta}{2}O_2 \tag{21}$$

where the extent of reduction δ, depends on the temperature and oxygen partial pressure, with both Δh_O and Δs_O having a dependence on δ (Panlener et al., 1975). Here we take analytical expressions for $\Delta h_O(\delta)$ and $\Delta s_O(\delta)$ (Bulfin et al., 2016), which are in good agreement with experimental literature sources (Panlener et al., 1975; Bevan and Kordis, 1964; Takacs et al., 2015). The equilibrium mole fractions of the products can then be determined for a range of non-stoichiometry δ. In order to calculate the product composition over a closed cycle between δ_{ox} and δ_{red} we must take the normalised average over δ for a given cycle,

$$\overline{x_i}(T,p) = \frac{\int_{\delta_{ox}}^{\delta_{red}} x_i(\delta,T,p)n_\delta(\delta,T,p)d\delta}{\sum_i \int_{\delta_{ox}}^{\delta_{red}} x_i(\delta,T,p)n_\delta(\delta,T,p)d\delta}. \tag{22}$$

The n_δ is to account for the fact that the amount of methane partially oxidised by the ceria changes with δ, due to the different amounts of oxygen in the equilibrium product composition, which changing the oxygen mass balance between the solid and gas phase. It is given by

$$n_\delta = \frac{1}{n_{CO} + n_{H_2O} + 2n_{CO2}}, \tag{23}$$

where it can be seen that H_2O and CO_2 formation lead to a smaller n_δ, which indicates that less methane is required for that δ. A similar integral can be performed for the number of moles of carbon, to determine the total carbon yield.

It's important to note that the non-stoichiometry introduces additional degrees of freedom in the cycle as there is a choice of the final oxidized and reduced non-stoichiometry, δ_{ox} and δ_{red} respectively.

2.1. Syngas composition

The formation of the products is the most important aspect of the reforming processes, which is examined by looking at the distribution of the species in the products. In addition to gas phase mole fractions, several unit-less metrics are applied to keep track of the mass balance. Firstly, the methane conversion extent, which is given by,

$$X_{CH_4} = 1 - \frac{n_{CH_4,\,f}}{n_{CH_4,\,0}}, \tag{24}$$

where $n_{CH_4,\,0}$ is the initial number of moles of methane, and $n_{CH_4,\,f}$ is the number of moles remaining after the reaction. We perform the mass balance for 1 mol of methane, so that the conversion extent is simplified to $X_{CH_4} = 1 - n_{CH_4,\,f}$.

Since we are interested in converting both the carbon in methane and carbon dioxide into carbon monoxide in the syngas, another important metric is the carbon monoxide yield which is given by,

$$Y_{CO} = \frac{n_{CO,\,f}}{n_{CH_4,\,0} + n_{CO2,\,0}}, \tag{25}$$

where again the subscript 0 indicates the initial moles and f indicates the final number of moles after the reactions.

The formation of solid phase carbon is reported using the carbon yield,

$$Y_C = \frac{n_{C,\,f}}{n_{CH_4,\,0} + n_{CO2,\,0}}. \tag{26}$$

which should be zero to ensure that carbon formation is not thermodynamically favourable.

Finally, for the redox cycles we are also interested in the conversion extent of the oxidation reaction given by,

$$X_{ox} = 1 - \frac{n_{H_2O,\,f} + n_{CO_2,\,f}}{n_{H_2O,\,0} + n_{CO_2,\,0}}. \tag{27}$$

2.2. Efficiency

An energy efficiency is defined to keep track of the energy balance for the system, which can be used to compare the thermodynamic performance of the different approaches of methane reforming. We define this as the higher heating value of the products, divided by the higher heating value of the feedstock and the solar heat input required by the reforming processes (Steinfeld, 2014),

$$\eta_{reforming} = \frac{HHV_{prod}}{HHV_{reac} + Q_{solar}}. \tag{28}$$

The solar heat input required by the reforming process is based off a simple process model illustrated in Fig. 4, and is given by,

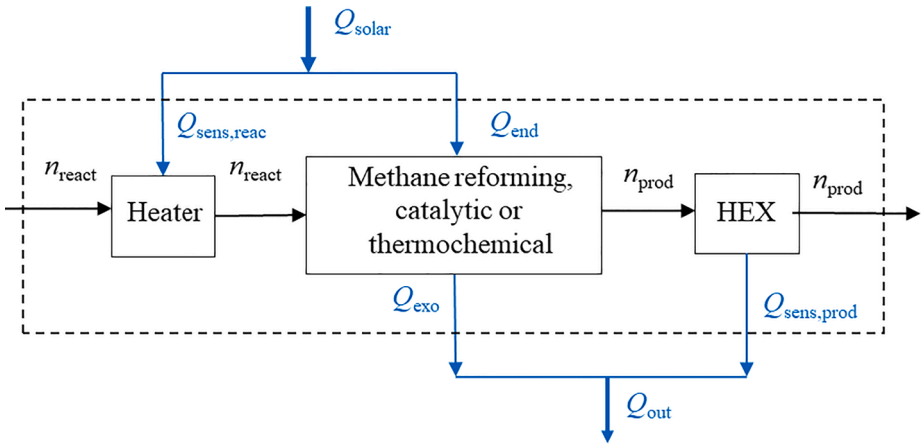

Fig. 4. A process schematic showing the key heat requirements and heat which can be recovered within the system. For the catalytic reforming $Q_{exo} = 0$. The unused heat Q_{out}, is high temperature process heat which could be utilized in a power block.

$$Q_{solar} = \frac{1}{\eta_{sol\ abs}}(Q_{end} + Q_{sens,reac}) \quad [kJ\,mol^{-1}], \tag{29}$$

where $\eta_{sol\ abs}$ is the solar absorption efficiency, Q_{end} is the heat required to drive the endothermic reaction, and $Q_{sens,reac}$ is the energy required to heat the reactants. This definition does not include the optical losses of the solar concentration system, but it is sufficient to get a relative comparison of the processes.

The solar absorption efficiency is determined using the Stefan Boltzmann law for a perfectly insulted black body solar receiver (only re-radiation losses) and is given by the equation,

$$\eta_{sol.\ abs.}(C,T) = 1 - \frac{\sigma(T^4)}{IC}, \tag{30}$$

where the solar concentration ratio C is defined as

$$C = \frac{\dot{Q}_{solar}}{IA}, \tag{31}$$

where $\dot{Q}_{solar}$ is the solar radiative power intercepted by the reactor aperture of area A, normalized to the direct normal solar irradiation I. C is often expressed in units of "suns". For all calculations the direct normal solar irradiation is taken to be 1 kW and the solar concentration ratio is set to $C = 2000$ suns.

The heat required to drive the endothermic reaction in catalytic reforming is simply given by the change in enthalpy due to the reaction given in Eq. (13),

$$Q_{end}(T,p) = H_{prod}(T,p) - H_{reac}(T,p) \tag{32}$$

For redox reforming it is the change in enthalpy due to the partial oxidation of methane given in Eq. (17) plus the enthalpy of reduction for the oxide,

$$Q_{end}(T,p) = H_{prod}(T,p) - H_{reac}(T,p) + 2n_{O_2}\Delta h_O. \tag{33}$$

The sensible heat of the reactants is given by,

$$Q_{sens,reac}(T,p) = H_{reac}(T,p) - H_{reac}(298\ K,p). \tag{34}$$

Our definition of $\eta_{reforming}$ is a simple metric to keep track of the relative energy demand of the system, without heat integration. There is also considerable amount of waste heat that could be utilized Q_{out}, which consists of the sensible heat in the products and in the case of redox reforming, it also contains the heat released in the exothermic oxidation reaction giving,

$$Q_{out} = Q_{sens,prod} + Q_{exo}. \tag{35}$$

$Q_{sens,prod}$ is the sensible heat in the product stream, and Q_{exo} is the energy released in the oxidation reaction. The heat released during oxidation of the metal oxide Q_{exo}, is the change in enthalpy due to the splitting of CO_2 and/or H_2O given in Eqs. (19) and (20) minus the enthalpy of reduction for the oxide,

$$Q_{exo}(T,p) = H_{prod}(T,p) - H_{reac}(T,p) - 2n_{O_2}\Delta h_O. \tag{36}$$

This waste heat Q_{out} is high temperature process heat, which in principle could be used to drive a power block (von Storch et al., 2016), or partially re-integrated into the reforming process using heat exchangers. Therefore, the efficiency results here are not a prediction of actual plant efficiencies, rather an approximation of relative energy demands.

3. Results

Most previous analysis of redox reforming have focused on operation at atmospheric pressure (Warren et al., 2017; Steinfeld et al., 1993; Steinfeld et al., 1995). However, natural gas is typically available at high pressures of up to 30 bar. Down-stream processing of the syngas, be it ammonia synthesis or GTL technologies, also requires high pressures greater than 30 bar. It is also standard in industrial applications to perform reforming at greater than atmospheric pressure. Here we consider the process to run at 15 bar, which is the value used in many industrial reforming plants (Bartholomew and Farrauto, 2011). This does have implications for the thermodynamics due to le Chateliers principle. To illustrate this we can look at the gas phase equilibrium constant of catalytic reforming and redox reforming, given by Eqs. (1) and (4), (5) respectively.

$$K_{catalytic} = \frac{p_{CO}p_{H_2}^3}{p_{CH_4}p_{H_2O}} \tag{37}$$

$$K_{reduction} = \frac{p_{CO}p_{H_2}^2}{p_{CH_4}} \tag{38}$$

$$K_{oxidation} = \frac{p_{H_2}}{p_{H_2O}} \tag{39}$$

We can see from these equilibrium constants that both catalytic reforming (Eq. (37)) and the reduction reaction (Eq. (38)) in redox reforming will be shifted to lower conversion extents if the pressure is increased, due to the greater number of moles of gas phase products. The oxidation reaction on the other hand will remain unchanged.

The lower conversion seen in the catalytic reforming and reduction reactions can be overcome by increasing the operating temperature or,

in the case of catalytic reforming by using excess steam, and thus shifting the equilibrium to favour conversion of methane to syngas.

3.1. Ceria non-stoichiometry

For redox reforming with ceria we must first consider an additional degree of freedom, which is the reduction extent δ. It is important to note that we only consider values of δ up to 0.25, similar to Warren et al. (2017), to avoid regions where phase transitions can occur. The equilibrium gas composition with respect to the ceria non-stoicheometry δ is shown in Fig. 5 at a temperature of 1323 K for both methane oxidation and combine H_2O and CO_2 splitting.

In the reduction step for $\delta < 0.05$ there is significant amounts of CO_2 and H_2O forming, and thus a poor carbon monoxide yield Y_{CO}, which is due to the fact that ceria more easily releases it's oxygen in this range (Panlener et al., 1975). The formation of these products has also been experimentally observed by Warren et al. (2017). In Table 2 of their work we can see that a cycle operating at 1 bar and 1120 °C shows a significant portion of H_2O and CO_2 in the products, which they attribute this to CH_4 coming into contact with excess ceria in the fixed bed reactor. For $\delta > 0.18$ we can see that carbon formation becomes favourable, as the oxide in this range is too difficult to reduce, and methane cracking becomes favourable. Similarly, when we look at the oxidation step, the yield of syngas is poor for $\delta < 0.05$, and carbon formation can be thermodynamically favourable for $\delta > 0.15$. Avoiding the formation of unwanted carbon at large δ, and CO_2 and H_2O at small δ, could be achieved by operating in the stoichiometry range δ, where the intrinsic oxide thermodynamics favour CO and H_2 formation.

When designing the cycle for a fixed bed system, one could control the stoichiometry limits after both oxidation and reduction, δ_{ox} and δ_{red}, by switching the gas flows at the appropriate times. The overall mole fractions in the products of a cycle are determined by the integral given in Eq. (22). The choice of δ_{ox} and δ_{red} can be used to optimize the methane conversion and the carbon monoxide yield. From Fig. 5, we can see that a pragmatic range of operation for the ceria cycle under the conditions plotted would be to use the range $\delta_{ox} - \delta_{red}$ of 0.1 −0.14. This range would offer a good compromise between methane conversion and carbon monoxide selectivity for a temperature of 1323 K.

3.2. Comparison of reforming routes

In the case of redox reforming, the cycles are modelled isothermally, where both the oxidation and reduction step take place at the same temperature. In practice, ideal isothermal operation may be challenging, as we have two reaction steps, one endothermic and one exothermic, with a net heat demand. The alternative idealised case would be to model the oxidation step as adiabatic, with the temperature increasing as the reaction proceeds. Heat integration from the oxidation step would allow for a more isothermal operation. The reality would be somewhere in between, and we choose the idealised isothermal case here as it allows for a simpler analysis, and comparison to catalytic reforming. An intentional temperature swing is also possible by actively cooling the oxide for the oxidation step, but this would introduce an additional energy demand and add complexity to the process. In a thermodynamic study by Holzemer et al. 2020, results can be seen for temperature swing cycles (Holzemer-Zerhusen et al., 2020).

We would like to have a final syngas composition suitable for conversion to liquid based fuels which requires a mixture of wet and dry reforming. To approximately achieve this and get an initial comparison of the reforming routes the reactant gas feeds were set according to Table 1. The feed ratios in the catalytic reforming case match those used in a methanol production plant in Iran methanol plant in Iran (Bartholomew and Farrauto, 2011; Holm-Larsen, 2001). In the redox reforming the oxidants are fed in a ratio $0.7H_2O{:}0.3CO_2$ to try and produce a similar syngas. Note that in the case of redox reforming the ratio CH_4: $H_2O{:}CO_2$ is not fixed as is the case in catalytic reforming. Instead, one mole of CH_4 was assumed to be supplied in the first step, and the amount of oxidants (H_2O and CO_2) required to re-oxidise the metal oxide were calculated based on conversion extents.

Fig. 6 shows the equilibrium results for catalytic reforming and the methane reduction of the metal oxides (i.e. reduction step of the redox refoming). In the case of zinc oxide, the low boiling point of zinc leads to a significant zinc vapour pressure in the gas phase. Zinc oxide is therefore not suitable for application in a fixed bed reactor, as the zinc would leave the reactor in the gas phase. We therefore moved the result for zinc oxide to the ESI. From Fig. 6 we can see for the remaining redox cycles,

Table 1
A table showing the reactants for the various cases analysed here.

Reforming route	Endothermic reactants	Exothermic reactants
Catalytic Reforming	CH_4+2.5H_2O + 0.3CO_2	-
Ceria cycle	CH_4 + $CeO_{1.9}$	0.7H_2O:0.3CO_2+$CeO_{1.9}$
Fe_3O_4 cycle	CH_4 + F_3O_4	0.7H_2O:0.3CO_2+ FeO
FeO cycle	CH_4 + FeO	0.7H_2O:0.3CO_2+ Fe
ZnO cycle	CH_4 +ZnO	0.7H_2O:0.3CO_2 + Zn

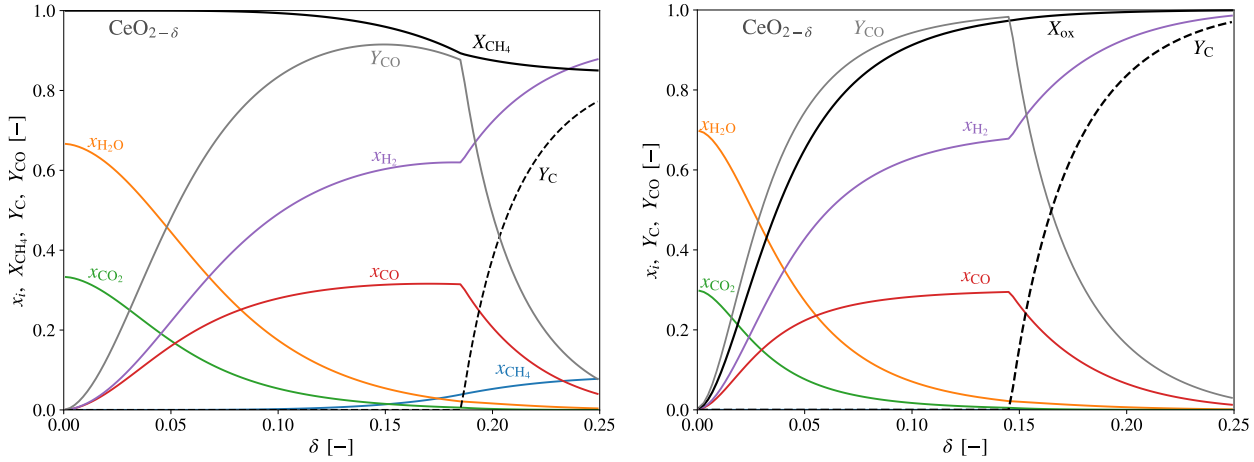

Fig. 5. Equilibrium gas mole fractions x_i, methane conversion extent X_{CH_4}, carbon monoxide yield Y_{CO} and solid carbon yield $Y_m athrmC$ of ceria vs. δ at a temperature of 1323 K and a pressure of 15 bar. **Left:** Equilibrium mole fractions of methane oxidation (Eq. (17)), with partial pressures of oxygen matching that of ceria, $p_{O_2}(\delta, T)$. **Right:** Equilibrium mole fractions for combined H_2O and CO_2 splitting in the ratio $0.7H_2O{:}0.3CO_2$, again with oxygen partial pressures matchin.g that of ceria.

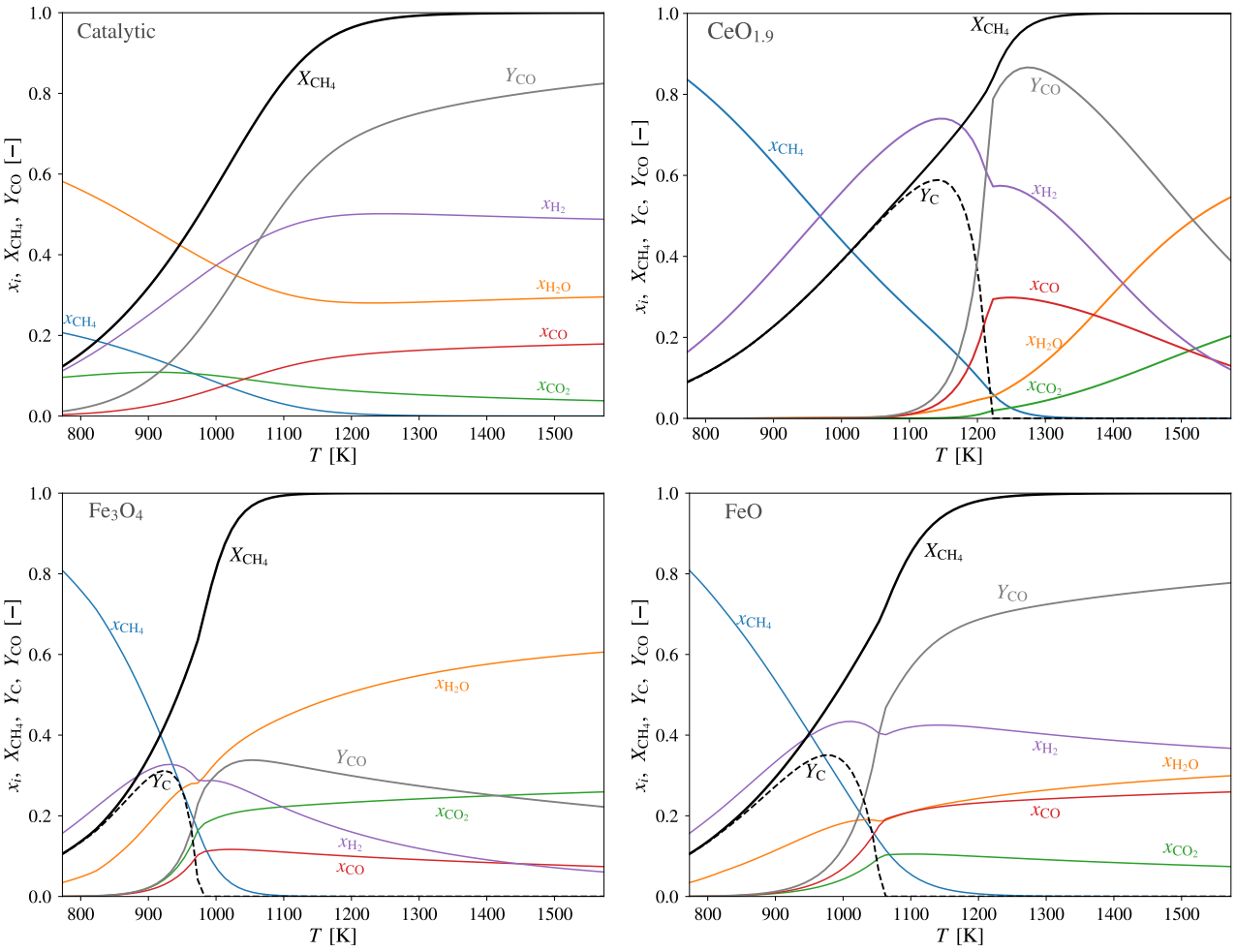

Fig. 6. Equilibrium gas mole fractions x_i, methane conversion extent X_{CH_4}, carbon monoxide yield Y_{CO} and solid carbon yield Y_C vs. temperature for catalyic reforming and the methane reduction reactions given in Table 1 at a pressure of 15 bar. Data for zinc oxide is g.iven in the ESI.

methane cracking to form carbon is favourable at low temperatures, which is avoided in the catalytic case due to the excess steam.

High methane conversion ($X_{CH_4} > 0.95$) is desirable for this processes, and from this perspective Fig. 6 shows that $CeO_{1.9}$ requires higher temperature than catalytic reforming and the reduction of iron oxides. This is due to the strong oxygen affinity of ceria requiring high temperature for reduction, which is in agreement with the Ellingham diagram given in Fig. 2. This will likely require the redox process with ceria to operate at greater temperatures than catalytic reforming.

From the perspective of carbon monoxide yield, $CeO_{1.9}$ does show the largest value at a temperature of approximately 1273 K, potentially offering a higher quality syngas than the catalytic case. Fe_3O_4 on the other hand shows a very poor carbon monoxide yield, due to it's ease of reduction allowing further oxidation to CO_2. This will also result in a low oxidation conversion extent. FeO improves upon this but the carbon monoxide yield is still bellow that of the catalytic reforming case. These result for iron oxides are supported by experimental demonstrations of Fe_3O_4 reduction with methane, where CO_2 has been observed as one of the main products (Steinfeld et al., 1993; Kang et al., 2008). In these experiments Fe_3O_4 is reduced first to FeO and then further reduced to Fe. In the first stages of reduction where Fe_3O_4 is reduced to FeO, CO_2 formation is seen to be dominant over CO. This agreement with experimental demonstrations highlights the value of using the oxygen activity model to determine the equilibrium composition of the gas, rather than the ideal stoichiometric modelling approach. This result means that the Fe_3O_4 cycle will result in a product stream containing relatively large amounts of CO_2, which will not be suitable for downstream processing.

To continue the analysis we focus on $CeO_{1.9}$ and FeO, which show better carbon monoxide yields.

Fig. 7 shows the oxidation equilibrium, where in terms of oxidation conversion extent $CeO_{1.9}$ shows the best performance, although at low temperature carbon formation is favourable. Chueh et al. found that an additional metal catalyst was required to observe carbon formation in this case (Chueh and Haile, 2009), and so it may be kinetically limited in practice. In any case, we require high temperature for the reduction step, and if the cycle is isothermal then the oxidation step will also be outside of the carbon formation region. The FeO/Fe cycle shows lower conversion and a lower carbon monoxide yield Y_{CO}. If we compare both the reduction and oxidation steps of the Fe/FeO cycle we see that this does not offer a better carbon monoxide yield compared to catalytic reforming. In any case, it is well known from thermochemical fuel production studies that the re-oxidation reaction of Iron oxides in H_2O and CO_2 in this process is problematic both kinetically and in terms of thermodynamic conversion extents (Miller et al., 2014). The process conditions are close to the melting points of the materials leading to significant degradation over time. CeO_2 on the other hand has been cycled over a thousands times at even high temperatures of 1773 K (Marxer et al., 2017).

From this analysis, ceria is the most pragmatic option from the redox cycles and it has been experimentally demonstrated as a closed cycle (Warren et al., 2017). The oxide does not undergo any phase changes, could offer high selectivity, and the syngas composition could be tuned by changing the oxidant ration H_2O:CO_2. Ceria has also been extensively investigated for thermochemical fuel production, with studies which

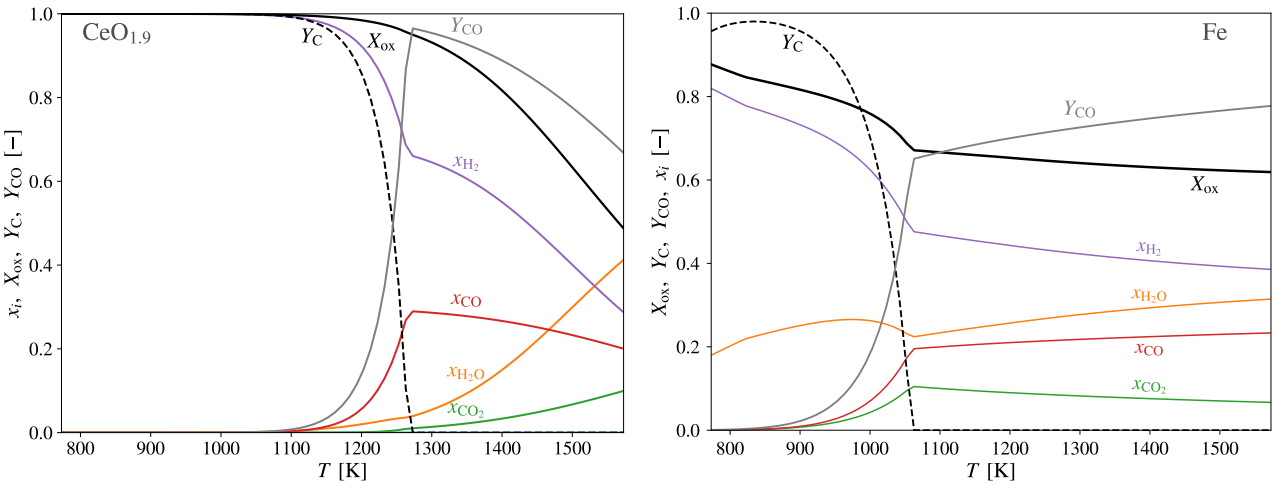

Fig. 7. Equilibrium gas mole fractions x_i, oxidation conversion extent X_{ox}, carbon monoxide yield Y_{CO} and solid carbon yield $Y_m athrmC$ vs. temperature for catalytic the oxidation of $CeO_{1.9}$ and Fe with an oxidant ratio of $0.7H_2O{:}0.3CO_2$, at a pressure of 15 bar.

highlight it's chemical stability and favourable kinetic properties (Marxer et al., 2017; Ackermann et al., 2014). We therefore focus the rest of the analysis on comparing CeO_2 to catalytic reforming, with the goal of producing syngas for gas to liquids processes.

4. Gas-to-liquid case study

Syngas itself is not a final product in high demand, but it can be used in other chemical processes such as hydrogen production, or conversion to a denser liquid fuel, which is preferable for storage, transportation and utilization. This can be achieved by either the Fischer–Tropsch process to produce hydrocarbon fuels or methanol synthesis (Bartholomew and Farrauto, 2011).

For the Fischer–Tropsch process the ratio of H_2 to CO in the syngas is important,

$$R_{H_2:CO} = \frac{x_{H_2}}{x_{CO}}, \tag{40}$$

with a value of 2.1 desirable. In the case of methanol synthesis, CO_2 can also be consumed, and so the stoichiometric module is used to determine the suitability of the syngas,

$$S = \frac{x_{H_2} - x_{CO_2}}{x_{CO} + x_{CO_2}}. \tag{41}$$

where the ideal stoichiometry is $S = 2$. In both cases large amounts of CO_2 in the syngas are undesirable as it shifts the equilibrium away from the desired products. This is illustrated in Fig. 8 where the equilibrium methanol yield Y_{CH_3OH}, is plotted for a range of syngas compositions.

$$Y_{CH_3OH} = \frac{n_{CH_3OH,f}}{n_{CO,0} + n_{CO_2,0}}. \tag{42}$$

From Fig. 8 it can be seen that the maximum thermodynamic yield for methanol synthesis is obtained at $2H_2{:}1CO$. Thermodynamics aside, CO_2 in the methanol synthesis feedstock can be tolerated, and indeed for some catalysts it has been observed to improve kinetics (Wender, 1996). A number of industrial methanol synthesis processes utilize syngas with a CO_2 content in the range of 4–8 %, and a stoichiometric module in the range $S = 2-2.1$ (Bartholomew and Farrauto, 2011).

Here we compare catalytic reforming to ceria redox reforming, with the goal of producing a syngas suitable for either methanol or Fischer–Tropsch synthesis. We set the following criteria for the processes:

- The methane conversion extent must be over 97 %, $X_{CH_4} > 0.97$.

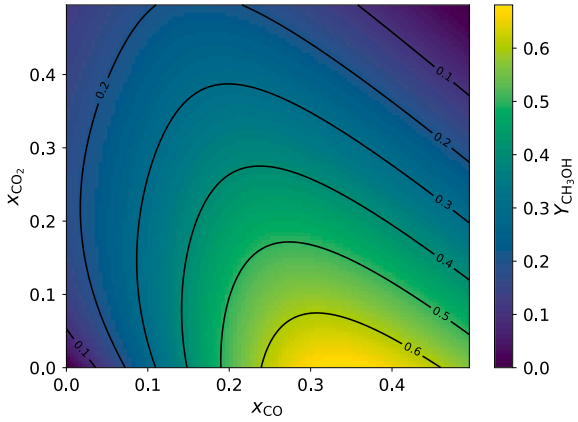

Fig. 8. Thermodynamic equilibrium mole fraction of methanol plotted against the mole fractions of CO and CO_2 in the syngas, at 500 K and 50 bar, with $x_{H_2} + x_{CO} + x_{CO_2} = 1$.

- There should be no carbon formation, $Y_C = 0$.
- For methanol synthesis we want a stoichiometric module of $S \approx 2.05$.
- For Fischer–Tropsch synthesis we want a syngas ratio of $R_{H_2:CO} \approx 2.1$.

In the case of catalytic reforming, the syngas composition can be adjusted by changing the amount of H_2O and CO_2 relative to CH_4, as well as the temperature of the reforming. In the case of the ceria cycle the amount of oxidants relative to CH_4 is fixed by the intrinsic thermodynamics of the oxide. However, we can adjust the ratio of the oxidants $H_2O{:}CO_2$, the range of non-stoicheometry δ, and the temperature of the reforming. From previous the results shown in Figs. 5–7, a delta range of $\delta = 0.1-0.14$ for the ceria cycle, as this avoids carbon formation and offers good carbon monoxide yield. The key results for a number of cases are shown in Table 2.

The relative feedstock ratios for the catalytic reforming case (i) shown in Table 2, were set to match a reforming case applied in the industry (Bartholomew and Farrauto, 2011; Holm-Larsen, 2001). The temperature and methane conversion extent also match the performance of that reforming process. This is a good validation of the thermodynamic model, where the high temperatures allowed the conversion extent to approach equilibrium. As well as this reforming composition we also looked at a large range of feedstock compositions for catalytic

Table 2
Results for catalytic reforming and the ceria cycle both at 15 bar, with the aim of using the syngas for down stream methanol synthesis, $S \approx 2.05$, or Fischer Tropsch (FT), $R_{H_2:CO} \approx 2.1$. In the case of $CeO_{2-\delta}$, the cycle stoichiometry range is $\delta_{ox} = 0.1$, and $\delta_{red} = 0.14$, with Eq. (22) used to calculate the product distribution averaged over the cycle.

Reforming GTL	Catalytic† (i) Methanol	Catalytic (ii) Methanol	$CeO_{2-\delta}$ (i) Methanol	Catalytic (iii) FT	$CeO_{2-\delta}$ (ii) FT
Temperature	1220 K	1280 K	1290 K	1290 K	1320 K
n_{H_2O}, n_{CO_2}	2.5, 0.3	1.6, 0.3	1.14, 0.3	1.0, 0.5	1.11, 0.39
X_{CH_4}	0.97	0.97	0.976	0.98	0.98
X_{ox}	-	-	0.95	-	0.95
Y_{CO}	0.72	0.84	0.91	0.81	0.91
$\eta_{refroming}$	0.77	0.79	0.7	0.78	0.7
x_{CO_2}	0.078	0.043	0.025	0.064	0.028
S	2.06	2.06	2.05	1.56	1.86
$R_{H_2:CO}$	3.13	2.54	2.31	2.12	2.12

† These catalytic reforming process conditions match those of in an industrial reforming to methanol plant in Iran (Bartholomew and Farrauto, 2011; Holm-Larsen, 2001).

reforming, with heat maps of the key results shown in the ESI. The results showed that the syngas composition could be tuned over a wide range of compositions at a temperature 1273 K and a pressure of 15 bar. From this analysis we selected catalytic reforming case (ii) in Table 2 for methanol synthesis, which offered a better carbon monoxide yield and lower CO_2 content. This second catalytic case also requires less oxidant feedstock, which would decrease sensible heat demand and flow rates, but it requires a higher temperature to achieve the desired methane conversion.

Comparing the catalytic reforming to the ceria reforming in Table 2, we can see that the ceria reforming does offer a larger carbon monoxide yield and a lower CO_2 content. On the other hand the ceria redox cycle has a lower efficiency, even though it requires lower amounts of oxidant feedstock, and thus has a lower sensible heating demand. This is because redox reforming has a larger enthalpy of reaction for the reduction step. The additional heat is released during the oxidation step, which leads to an overall greater energy demand.

The decrease in efficiency seen for the ceria redox cycle compared to catalytic reforming is not specific to ceria. A redox cycle introduces additional thermodynamic constraints, where in order to get good conversion of the oxidants, the oxidation reaction must be relatively exothermic (Bulfin et al., 2017). The result is that the process will have a portion of waste heat from the oxidation. Some of this heat loss could be avoided, using heat integration, particularly in the case of the ceria cycle. The large heat capacity of the ceria bed ($\frac{1}{\Delta\delta} C_{p,CeO_2}$), could also absorb some of the oxidation heat and re-release it during the reduction step. However, the details of this energy balance would depend on the reactor design. Further assessing the efficiency would require a reactor design study.

Similarly, when we consider Fischer–Tropsch synthesis the ceria cycle case (ii) offers a better carbon monoxide yield and lower CO_2 content relative to the catalytic reforming case (iii), but again with a lower efficiency. In this case the ceria cycle temperature had to be increased to avoid carbon formation in the oxidation step, as we now have more CO_2 in the feed. This sensitivity to carbon formation may be a considerable drawback to redox reforming. This problem is more acute at a pressure of 15 bar, than at 1 bar where the previous analysis by Warren et al. (2017) was performed.

Sensitivity to carbon formation may be of critical importance for this process, not just for the reforming conditions, but also for the heating of the feedstock. For redox reforming pure methane makes up the feedstock, and so during the heating of this feedstock carbon formation via methane cracking will be thermodynamically favourable. For the catalytic cases in Table 2 we performed a thermodynamic equilibrium calculation of feedstock vs. temperature to check the possibility of carbon formation during the heating of the feedstock, with the results plotted in the ESI. Only case (iii) showed favourable carbon formation, and for temperatures below 800 K, where it will likely be kinetically limited without a catalyst. Therefore, to help avoid carbon formation, the reactants should enter the catalytic reactor above 800 K.

Although the ceria cycle does offer a slight performance increase in terms of syngas quality, it comes with a greater energy demand, and a narrow window of operation to avoid carbon formation. The thermodynamics of mixed catalytic reforming on the other hand do show good flexibility in terms of tuning the syngas composition, and a lower energy demand. It is also important to note that catalytic reforming is a single step continous flow process which is more industrially mature, compared to the ceria cycle which has been proposed in the literature, with only small scale experimental demonstrations at atmospheric pressure (Warren et al., 2017; Welte et al., 2017; Nair and Abanades, 2016; Fosheim et al., 2019).

The option of using CSP heat directly in a chemical process to upgrade natural gas to a liquid fuel product, could be an intermediate step in decreasing consumption of CO_2 releasing fossil fuels. The resulting fuel has been produced partly by solar energy which is reflected in the consumption of CO_2 in the process. Such a plant could have a hybrid operation, using natural gas for heat in the dark hours, and also combine some CSP heat storage to maximise the solar input.

5. Conclusions

The thermodynamic analysis presented shows the theoretical limitations of a number of routes considered for solar methane reforming for a GTL plant. The results show that the industrial standard of direct catalytic reforming has good underlying thermodynamics, and with mixed reforming could offer a promising route to hybrid solar methanol or hydrocarbons via Fischer–Tropsch. Thermodynamic calculations also suggest that redox reforming using the ceria cycle could offer a high quality syngas composition, but with a sensitivity to carbon formation and a larger energy demand.

Declaration of Competing Interest

The authors have financial interests in the company Synhelion.

Acknowledgements

We gratefully acknowledge the financial support of the Swiss Federal office of Energy (Project HYBREC – Grant No. SI/501854-01) and of the European Union's Horizon 2020 Research Infrastructure Programme (Project SFERA-III – Grant Nr. 823802).

Appendix A. Supplementary material

Supplementary data associated with this article can be found, in the online version, at https://doi.org/10.1016/j.solener.2020.11.076.

References

Ackermann, S., Scheffe, J.R., Steinfeld, A., 2014. Diffusion of oxygen in ceria at elevated temperatures and its application to H_2O/CO_2 splitting thermochemical redox cycles. J. Phys. Chem. C 118 (10), 5216–5225.
Agrafiotis, C., von Storch, H., Roeb, M., Sattler, C., 2014. Solar thermal reforming of methane feedstocks for hydrogen and syngas production-a review. Renew. Sustain. Energy Rev. 29, 656–682.
Bale, C., Chartrand, P., Degterov, S., Eriksson, G., Hack, K., Mahfoud, R.B., Melançon, J., Pelton, A., Petersen, S., 2002. FactSage thermochemical software and databases. Calphad 26 (2), 189–228.
Bale, C., Bélisle, E., Chartrand, P., Decterov, S., Eriksson, G., Hack, K., Jung, I.-H., Kang, Y.-B., Melançon, J., Pelton, A., et al., 2009. FactSage thermochemical software and databases-recent developments. Calphad 33 (2), 295–311.

Bartholomew, C.H., Farrauto, R.J., 2011. Fundamentals of Industrial Catalytic Processes. John Wiley & Sons.
Berman, A., Karn, R.K., Epstein, M., 2007. Steam reforming of methane on a Ru Al_2O_3 catalyst promoted with Mn oxides for solar hydrogen production. Green Chem. 9 (6), 626–631.
Bevan, D., Kordis, J., 1964. Mixed oxides of the type MO_2 (fluorite)-M_2O_3 oxygen dissociation pressures and phase relationships in the system CeO_2 - Ce_2O_3 at high temperatures. J. Inorg. Nucl. Chem. 26 (9), 1509–1523.
Buck, R., Muir, J.F., Hogan, R.E., 1991. Carbon dioxide reforming of methane in a solar volumetric receiver/reactor: the CAESAR project. Sol. Energy Mater. 24 (1–4), 449–463.
Bulfin, B., Hoffmann, L., de Oliveira, L., Knoblauch, N., Call, F., Roeb, M., Sattler, C., Schmuecker, M., 2016. Statistical thermodynamics of non-stoichiometric ceria and ceria zirconia solid solutions. PCCP 18 (33), 23147–23154.
Bulfin, B., Vieten, J., Agrafiotis, C., Roeb, M., Sattler, C., 2017. Applications and limitations of two step metal oxide thermochemical redox cycles; a review. J. Mater. Chem. A 5 (36), 18951–18966.
Chueh, W.C., Haile, S.M., 2009. Ceria as a thermochemical reaction medium for selectively generating syngas or methane from H_2O and CO_2. ChemSusChem: Chem. Sustainab. Energy Mater. 2 (8), 735–739.
Diver, R., Fish, J., Levitan, R., Levy, M., Meirovitch, E., Rosin, H., Paripatyadar, S., Richardson, J., 1992. Solar test of an integrated sodium reflux heat pipe receiver/reactor for thermochemical energy transport. Sol. Energy 48 (1), 21–30.
Ehrensberger, K., Palumbo, R., Larson, C., Steinfeld, A., 1997. Production of carbon from carbon dioxide with iron oxides and high-temperature solar energy. Ind. Eng. Chem. Res. 36 (3), 645–648.
Fosheim, J.R., Hathaway, B.J., Davidson, J.H., 2019. High efficiency solar chemical-looping methane reforming with ceria in a fixed-bed reactor. Energy 169, 597–612.
Goodwin, D., Moffat, H., Speth, R., 2017. Cantera: An Object-Oriented Software Toolkit for Chemical Kinetics, Thermodynamics, and Transport Processes, Version 2.3. 0, doi:10.5281/zenodo. 170284.
Halmann, M., Frei, A., Steinfeld, A., 2002. Thermo-neutral production of metals and hydrogen or methanol by the combined reduction of the oxides of zinc or iron with partial oxidation of hydrocarbons. Energy 27 (12), 1069–1084.
He, F., Li, F., 2015. Perovskite promoted iron oxide for hybrid water-splitting and syngas generation with exceptional conversion. Energy Environ. Sci. 8 (2), 535–539.
He, F., Trainham, J., Parsons, G., Newman, J.S., Li, F., 2014. A hybrid solar-redox scheme for liquid fuel and hydrogen coproduction. Energy Environ. Sci. 7 (6), 2033–2042.
Holm-Larsen, H., 2001. CO_2 reforming for large scale methanol plants-an actual case. Stud. Surf. Sci. Catal 136, 441–446.
Holzemer-Zerhusen, P., Brendelberger, S., von Storch, H., Roeb, M., Sattler, C., Pitz-Paal, R., 2020. Efficiency assessment of solar redox reforming in comparison to conventional reforming. Int. J. Hydrogen Energy 45 (7), 4137–4151.
Kang, K.-S., Kim, C.-H., Cho, W.-C., Bae, K.-K., Woo, S.-W., Park, C.-S., 2008. Reduction characteristics of CuFe_2O_4 and Fe_3O_4 by methane; CuFe_2O_4 as an oxidant for two-step thermochemical methane reforming. Int. J. Hydrogen Energy 33 (17), 4560–4568.
Kodama, T., Ohtake, H., Matsumoto, S., Aoki, A., Shimizu, T., Kitayama, Y., 2000. Thermochemical methane reforming using a reactive WO_3/W redox system. Energy 25 (5), 411–425.
Kräupl, S., Steinfeld, A., 2001. Experimental investigation of a vortex-flow solar chemical reactor for the combined ZnO-reduction and CH_4-reforming. J. Sol. Energy Eng. 123 (3), 237–243.
Krenzke, P.T., Davidson, J.H., 2014. Thermodynamic analysis of syngas production via the solar thermochemical cerium oxide redox cycle with methane-driven reduction. Energy Fuels 28 (6), 4088–4095.
Krenzke, P.T., Fosheim, J.R., Zheng, J., Davidson, J.H., 2016. Synthesis gas production via the solar partial oxidation of methane-ceria redox cycle: Conversion, selectivity, and efficiency. Int. J. Hydrogen Energy 41 (30), 12799–12811.
Marxer, D., Furler, P., Takacs, M., Steinfeld, A., 2017. Solar thermochemical splitting of CO_2 into separate streams of CO and O_2 with high selectivity, stability, conversion, and efficiency. Energy Environ. Sci.
Miller, J.E., McDaniel, A.H., Allendorf, M.D., 2014. Considerations in the design of materials for solar-driven fuel production using metal-oxide thermochemical cycles. Adv. Energy Mater. 4 (2).
Muir, J.F., Hogan Jr, R.E., Skocypec, R.D., Buck, R., 1994. Solar reforming of methane in a direct absorption catalytic reactor on a parabolic dish: I—Test and analysis. Sol. Energy 52 (6), 467–477.
Muraza, O., Galadima, A., 2015. A review on coke management during dry reforming of methane. Int. J. Energy Res. 39 (9), 1196–1216.
Nair, M.M., Abanades, S., 2016. Tailoring hybrid nonstoichiometric ceria redox cycle for combined solar methane reforming and thermochemical conversion of H_2O/CO_2. Energy Fuels 30 (7), 6050–6058.
Otsuka, K., Ushiyama, T., Yamanaka, I., 1993. Partial oxidation of methane using the redox of cerium oxide. Chem. Lett. 22 (9), 1517–1520.
Otsuka, K., Wang, Y., Sunada, E., Yamanaka, I., 1998. Direct partial oxidation of methane to synthesis gas by cerium oxide. J. Catal. 175 (2), 152–160.
Panlener, R., Blumenthal, R., Garnier, J., 1975. A thermodynamic study of nonstoichiometric cerium dioxide. J. Phys. Chem. Solids 36 (11), 1213–1222. https://doi.org/10.1016/0022-3697(75)90192-4. ISSN 0022-3697.
Romero, M., Steinfeld, A., 2012. Concentrating solar thermal power and thermochemical fuels. Energy Environ. Sci. 5 (11), 9234–9245.
Rostrup-Nielsen, J.R., Sehested, J., Nørskov, J.K. 2002. Hydrogen and synthesis gas by steam-and CO_2 reforming.
Segal, A., Epstein, M., 2003. Solar ground reformer. Sol. Energy 75 (6), 479–490.
Sheu, E.J., Mokheimer, E.M., Ghoniem, A.F., 2015. A review of solar methane reforming systems. Int. J. Hydrogen Energy 40 (38), 12929–12955.
Smith, W.R., 1982. Chemical reaction equilibrium analysis. Theory Algorith.
Steinfeld, A., 1997. High-temperature solar thermochemistry for CO_2 mitigation in the extractive metallurgical industry. Energy 22 (2–3), 311–316.
Steinfeld, A., 2014. Solar Thermochemical Production of Hydrogen, Handbook of Hydrogen Energy, CRC Press, ISBN 978-1-4200-5447-7.
Steinfeld, A., Thompson, G., 1994. Solar combined thermochemical processes for CO_2 mitigation in the iron, cement, and syngas industries. Energy 19 (10), 1077–1081.
Steinfeld, A., Kuhn, P., Karni, J., 1993. High-temperature solar thermochemistry: production of iron and synthesis gas by Fe_3O_4-reduction with methane. Energy 18 (3), 239–249.
Steinfeld, A., Frei, A., Kuhn, P., Wuillemin, D., 1995. Solar thermal production of zinc and syngas via combined ZnO-reduction and CH_4-reforming processes. Int. J. Hydrogen Energy 20 (10), 793–804.
Steinfeld, A., Kuhn, P., Reller, A., Palumbo, R., Murray, J., Tamaura, Y., 1998. Solar-processed metals as clean energy carriers and water-splitters. Int. J. Hydrogen Energy 23 (9), 767–774.
Takacs, M., Scheffe, J., Steinfeld, A., 2015. Oxygen nonstoichiometry and thermodynamic characterization of Zr doped ceria in the 1573–1773 K temperature range. Phys. Chem. Chem. Phys. 17 (12), 7813–7822.
von Storch, H., Roeb, M., Stadler, H., Sattler, C., Bardow, A., Hoffschmidt, B., 2016. On the assessment of renewable industrial processes: Case study for solar co-production of methanol and power. Appl. Energy 183, 121–132.
Warren, K.J., Reim, J., Randhir, K., Greek, B., Carrillo, R., Hahn, D.W., Scheffe, J.R., 2017. Theoretical and experimental investigation of solar methane reforming through the nonstoichiometric ceria redox cycle. Energy Technol. 5 (11), 2138–2149.
Welte, M., Warren, K., Scheffe, J.R., Steinfeld, A., 2017. Combined ceria reduction and methane reforming in a solar-driven particle-transport reactor. Ind. Eng. Chem. Res. 56 (37), 10300–10308.
Wender, I., 1996. Reactions of synthesis gas. Fuel Process. Technol. 48 (3), 189–297.
Zedtwitz, P., Petrasch, J., Trommer, D., Steinfeld, A., 2006. Hydrogen production via the solar thermal decarbonization of fossil fuels. Sol. Energy 80 (10), 1333–1337.